

Available online at www.sciencedirect.com





journal homepage: www.elsevier.com/locate/jmrt

Short Communication

Multimodal analysis and characterization of the boehmite layer formed on AA6061 before and after alkaline etching



Lyndi E. Strange ^{a,*}, Vaithiyalingam Shutthanandan ^b, Miao Song ^c, Mark Bowden ^c, Quin R.S. Miller ^c, Ramprashad Prabhakaran ^a, Rick Shimskey ^a, Vineet V. Joshi ^{a,**}

ARTICLE INFO

Article history: Received 15 July 2022 Accepted 29 September 2022 Available online 5 October 2022

Keywords:
Boehmite
AA6061
XPS
U-10Mo
Multimodal analysis

ABSTRACT

Low-enriched uranium (LEU) alloyed with 10% Mo (U-10Mo) is being considered as a promising alternative to oxide-based dispersion fuel with high-enriched uranium for use in research reactors. The configuration of this proposed LEU monolithic LEU fuel plate consists of a U-10Mo plate-type fuel foil with a 25 μ m zirconium interlayer barrier clad with an aluminum alloy (AA6061). In certain research reactors, the clad AA6061 is coated with a boehmite layer to prevent corrosion. The boehmite layer has a high-pH passivation range, which makes it resistant to oxidation. Boehmite is usually formed on the AA6061 surface by autoclave processing. Before the boehmite layer is added, the surface of the AA6061 is cleaned using techniques such as polishing and wet etching. In this study, we use multimodal analysis to examine how pretreatment of AA6061 using polishing followed by alkaline etching affects the chemical composition of the boehmite layer. X-ray photoelectron microscopy (XPS), transmission electron microscopy (TEM), and x-ray diffraction (XRD) were used to study the chemical changes in the boehmite layer caused by alkaline etching pretreatment. XPS provides quantitative analysis for the Al:O ratio as well as oxidation states present on the surface, which suggests slight oxidation of the boehmite surface after alkaline etching of the AA6061 surface. We further explored this suggested oxidation of the boehmite surface using high-resolution transmission electron microscopy with selected area electron diffraction (SAED) and grazing incidence x-ray diffraction (GI-XRD), which suggested only a small amount of aluminum oxide at the surface. The multimodal analysis and imaging yielded new insights for optimizing boehmite growth on AA6061 for research reactors.

© 2022 Elsevier B.V. This is an open access article under the CC BY-NC-ND license (http://creativecommons.org/licenses/by-nc-nd/4.0/).

^a Energy and Environment Directorate, Pacific Northwest National Laboratory

^b Environmental Molecular Sciences Laboratory, Pacific Northwest National Laboratory

^c Physical and Computational Sciences Directorate, Pacific Northwest National Laboratory

^{*} Corresponding author.

^{**} Corresponding author.

1. Introduction

Low-enriched uranium alloyed with 10 wt% molybdenum (U-10Mo) has been identified as a promising alternative to highly enriched uranium for the United States High Performance Research Reactors [1—3]. These research reactors are designed to operate over a wide range of core power densities, which can be as much as 30 times that of a conventional pressurized water reactor and provide a high neutron flux (exceeding commercial reactors) for applications such as neutron scattering and isotope production [4]. Therefore, designing materials that can withstand the power levels required is vital for reactor performance. Uranium-molybdenum (U-Mo) alloys have received much attention because they incur little swelling and offer geometric stability and mechanical integrity at high ratios of power density to fission density, which makes them promising materials for use in research reactors [5].

The nominal configuration of the low-enriched U-10Mo plate-type fuel is a metallic U-10Mo fuel foil enriched to slightly less than 20% 235 U, the thickness of which varies from 0.6 mm to 0.25 mm depending on the reactor; a 25 μm thick zirconium interlayer on either side; and a relatively thick outer cladding of AA6061 aluminum [6,7]. Aluminum is used because it has a high corrosion resistance due to the stable oxide layer that forms at the surface. The oxide layer will disappear when exposed to conditions that disrupt it, such as high temperature and pressure and low pH, which are common in a typical fuel configuration. Furthermore, it has been shown that thick oxide layer present on the Al cladding on research reactors have several detrimental effects on fuel performance due to the lower thermal conductivity of the oxide [8]. The possible reactions of Al with water are as follows [9]:

$$2Al + 6H_2O \rightarrow 2Al(OH)_3 + 3H_2$$
 (1)

$$2Al + 4H2O \rightarrow 2AlOOH + 3H2$$
 (2)

$$2Al + 3H_2O \rightarrow Al_2O_3 + 3H_2$$
 (3)

The products resulting from corrosion of the Al surface are aluminum oxide (Al₂O₃), bayerite [Al(OH)₃] and

aluminum hydroxide boehmite (AlOOH). Furthermore, the dominance of stable aluminum oxide products depends on the reaction temperature. Secondary reactions can also occur with the oxide products to produce gibbsite (γ -Al(OH)₃) and bayerite (α -Al(OH)₃), depending on the pH and temperature. Boehmite (γ -AlOOH) will form between 102 °C and 400 °C. In fact, the growth of the various oxides is largely dependent on three factors: (1) heat flux, (2) flow rate, and (3) pH of the coolant [10]. Presence of an oxide layer has been shown to decrease reactor performance [11]. However, boehmite exhibits a large passivation pH range of 4.7-6.2, where it also has good water resistance [12,13]. Therefore, boehmite formation on top of the aluminum cladding is used to increase corrosion resistance of the AA6061 surface to unwanted aluminum oxide-containing products such as Al₂O₃ and Al(OH)₃. The protective layer of boehmite is usually 1.5 μ m-7.6 μ m thick [14,15]. To produce a quality boehmite layer, the AA6061 is usually pretreated by polishing and cleaning. The cleaning process or treatment method can involve alkaline etching of the AA6061 coupon after polishing (shown in Fig. 1). Previous work has shown that the pretreatment methods do not affect the final surface roughness of the final boehmite layer [16]. However, the chemical properties and morphological characteristics of the boehmite layer have yet to be investigated. The etching treatments likely affect the nucleation sites where boehmite forms on the AA6061 surface. The theorized reaction of boehmite growth in an autoclave is $Al_2O_3 + H_2O \rightarrow 2AlOOH$ on top of the AA6061 surface. The alkaline etching treatment likely removes some of the oxide layer, which could expose more nucleation sites for boehmite growth. Alternatively, the presence of OH⁻ anions could result in unwanted oxidation of the boehmite layer. Thus, the goal of this work is to thoroughly investigate how alkaline pretreatment affects the boehmite layer on top of the AA6061 cladding.

In the current work, surface analytical techniques such as x-ray photoelectron microscopy (XPS), transmission electron microscopy (TEM), and x-ray diffraction (XRD) are used to study how the surface pretreatment method chemically affects the boehmite layer on AA6061. The information obtained from these surface-sensitive and high-resolution microanalysis techniques can provide a more complete knowledge of the boehmite chemical and morphological changes that the surfaces undergo as a result of AA6061 pretreatment.

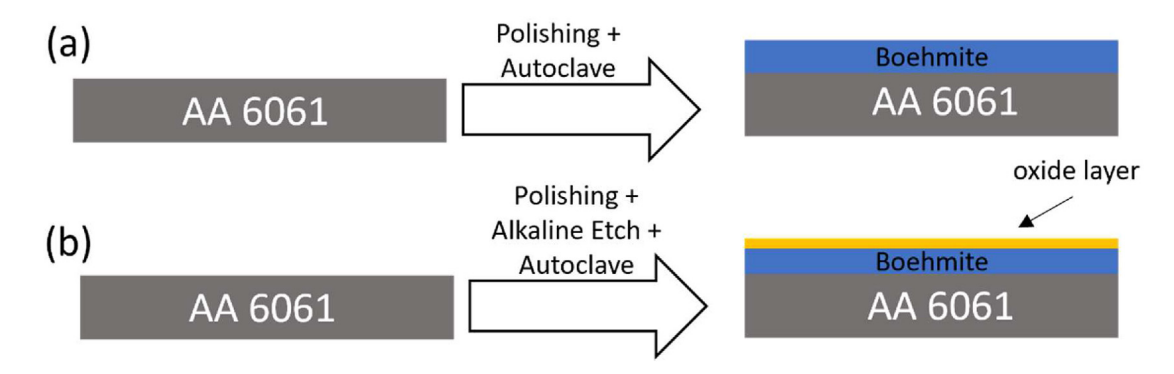


Fig. 1 – Schematic of sample preparation for the (a) polished boehmite and (b) alkaline-etched boehmite coupons.

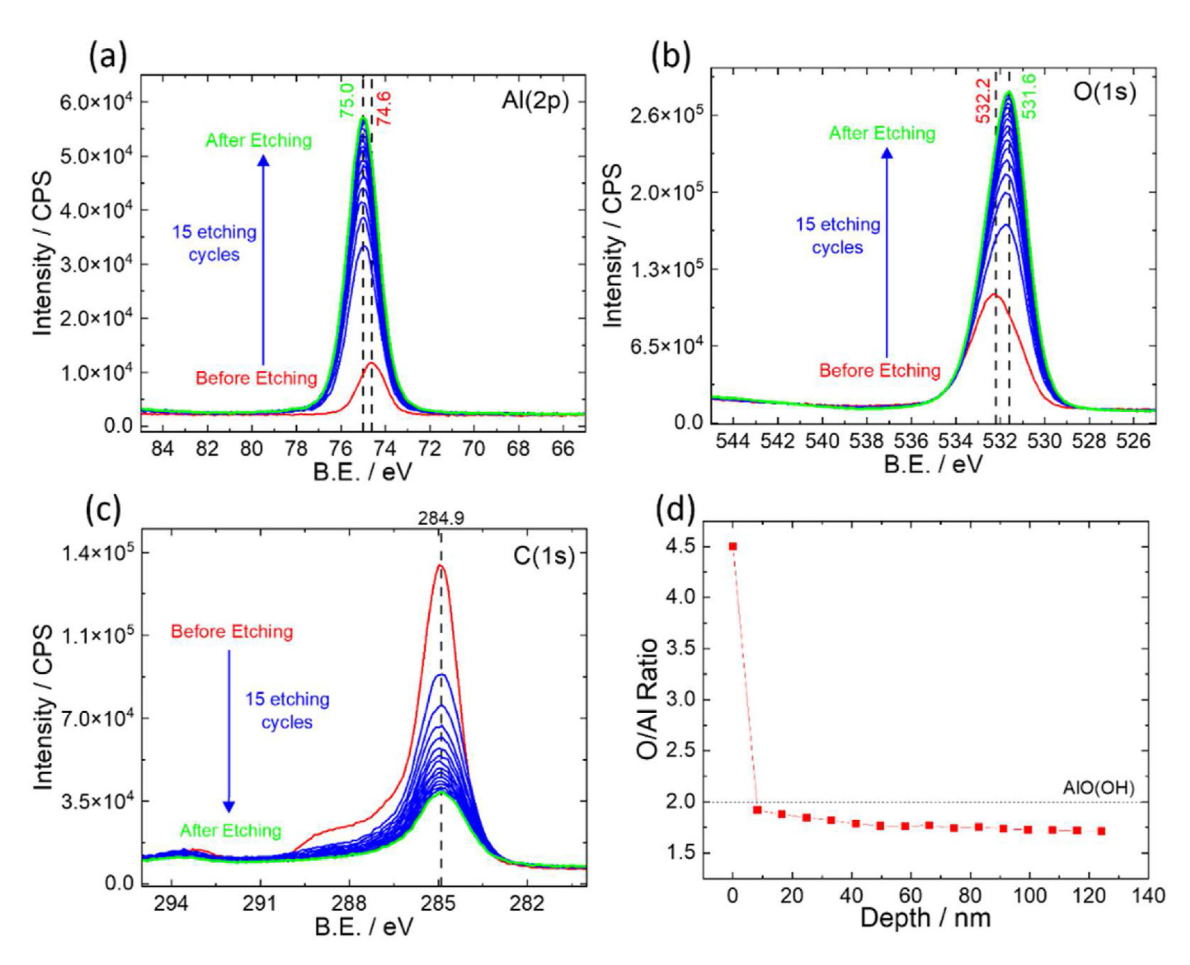


Fig. 2 – XPS depth profiling measurements for the alkaline pretreated boehmite sample with narrow scan regions: (a) Al(2p), (b) O(1s), (c) C(1s), and (d) peak area ratios of O to Al.

2. Methods

2.1. Boehmite coupon preparation

Dry polishing of the AA6061 substrates was performed using a Grade A45 belt provided by 3 M Inc. to remove scratches followed by a rinse with IPA. Another round of polishing was performed after with a Grade A30 belt to provide the final plate finish. The "alkaline" treated sample was etched with Oakite prior to boehmite growth whereas the "polished" sample was not treated post-polishing. The boehmite layer on the Al coupons was prepared by treatment of an AA6061 polished and then etched (for the alkaline sample) in Oakite inside an autoclave with 0.1 M NaOH (adjusted to pH 8). The autoclave vessel was placed in an oven that was ramped to 185 °C for 2 h and held for 18 h.

2.2. X-ray photoelectron spectroscopy (XPS)

XPS was used to determine the surface composition and chemical state of elements in the polished and alkaline treated aluminum coupons. The aluminum coupons were mounted on a sample holder using double-sided copper (Cu) tape and the XPS measurements were performed using a

Thermo Fisher Scientific Nexsa spectrometer, which consists of a high-performance, focused Al Kα monochromatic x-ray source (1486.6 eV) and a high-resolution spherical mirror analyzer. The x-ray source was operated at 72 W and the emitted photoelectrons were collected at the analyzer entrance slit normal to the sample surface. The data acquisition was carried out using a 400 µm diameter x-ray beam. The survey spectra were recorded at a pass energy of 160 eV with 0.5 eV step size, and high-resolution spectra were recorded at a pass energy of 50 eV with step size of 0.1 eV. The chamber pressure was maintained at $\sim 5 \times 10^{-9}$ Torr during the measurements. All the XPS peaks were charge-referenced using C 1s binding energy at 285 eV. XPS data were analyzed by CasaXPS software using Shirley background subtraction. For depth profile measurement, 500 eV monoenergetic argon ions were used. The ion beam was rastered over an area of about $1.2 \text{ mm} \times 1.2 \text{ mm}$ and the XPS measurements were performed at the center of the crater using a 400 μm diameter x-ray beam. The sputter time was converted into depth using Ta₂O₅ sputter rates.

2.3. Transmission electron microscopy (TEM)

The cross-section TEM specimen was prepared by the focused-ion-beam (FIB) lift-out technique using a gallium (Ga)-

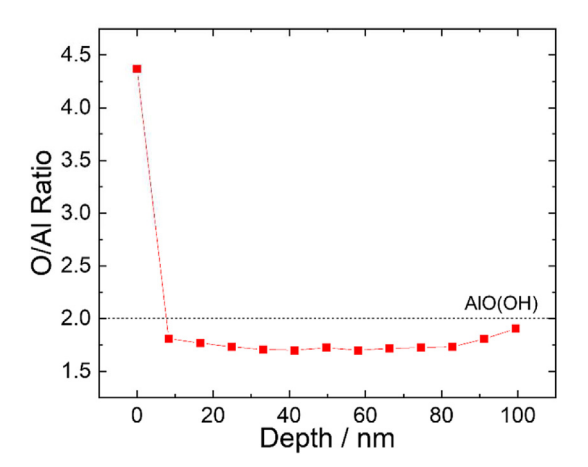


Fig. 3 - O(1s):Al(2p) integrated peak area ratio for the polished boehmite coupon.

based FIB scanning electron microscope (FIB-SEM, Helios NanoLab 600i, Thermo Fisher Scientific, USA). An aberration-corrected environmental transmission electron microscope (Thermo Fisher Scientific, USA) was employed at 300 kV for the bright-field (BF) image and SAED pattern.

2.4. Grazing incidence x-ray diffraction (GI-XRD)

Grazing incidence XRD patterns were collected using a Rigaku SmartLab XE diffractometer equipped with a 9 kW rotating Cu x-ray source. A parallel beam from a multilayer x-ray mirror passed through a 0.2 mm slit before making an incident angle of 1° with the sample surface. Diffraction data were collected

between 5 and 80 $^{\circ}2\theta$ at 0.02° intervals, scanning at 0.5 $^{\circ}2\theta/$ min. Compounds were identified through comparison with reference patterns from the ICDD (PA, USA).

3. Results

3.1. X-ray photoelectron spectroscopy

To identify the suggested oxidation of the polished and alkaline-etched XPS was used because it can identify chemical oxidation states on a surface. Fig. 2 shows the XPS depthprofile spectra for the alkaline treated boehmite sample. Fig. 2a shows the aluminum Al(2p) peak position during the etching cycle. Before etching, the Al(2p) peak is centered around 74.5 eV, which indicates that Al₂O₃ and Al(OH)₃ are present and likely part of a thicker oxidation layer at the surface [17-20]. However, the peak resolution to distinguish Al₂O₃ is less than 0.5 eV, which makes it difficult to resolve peak components. However, the peak does shift to a higher binding energy after etching to 75 eV, which is consistent with the binding energy reported for boehmite [21]. The O(1s) peak in the polished boehmite coupon shifts to a lower binding energy during the etching cycle; this could be a result of metal carbonate and other carbon related contaminants (hydrocarbon residues possibly from the alkaline cleaner) [22] present on the sample that are etched away after the first cycle, leaving a higher concentration of aluminum oxide and hydroxide present. The reported binding energies for aluminum oxide, hydroxide, and boehmite are all around 531.8 eV [17-20], and it is difficult to resolve individual contributions of each oxide product. Fig. 2c shows an adventitious carbon peak

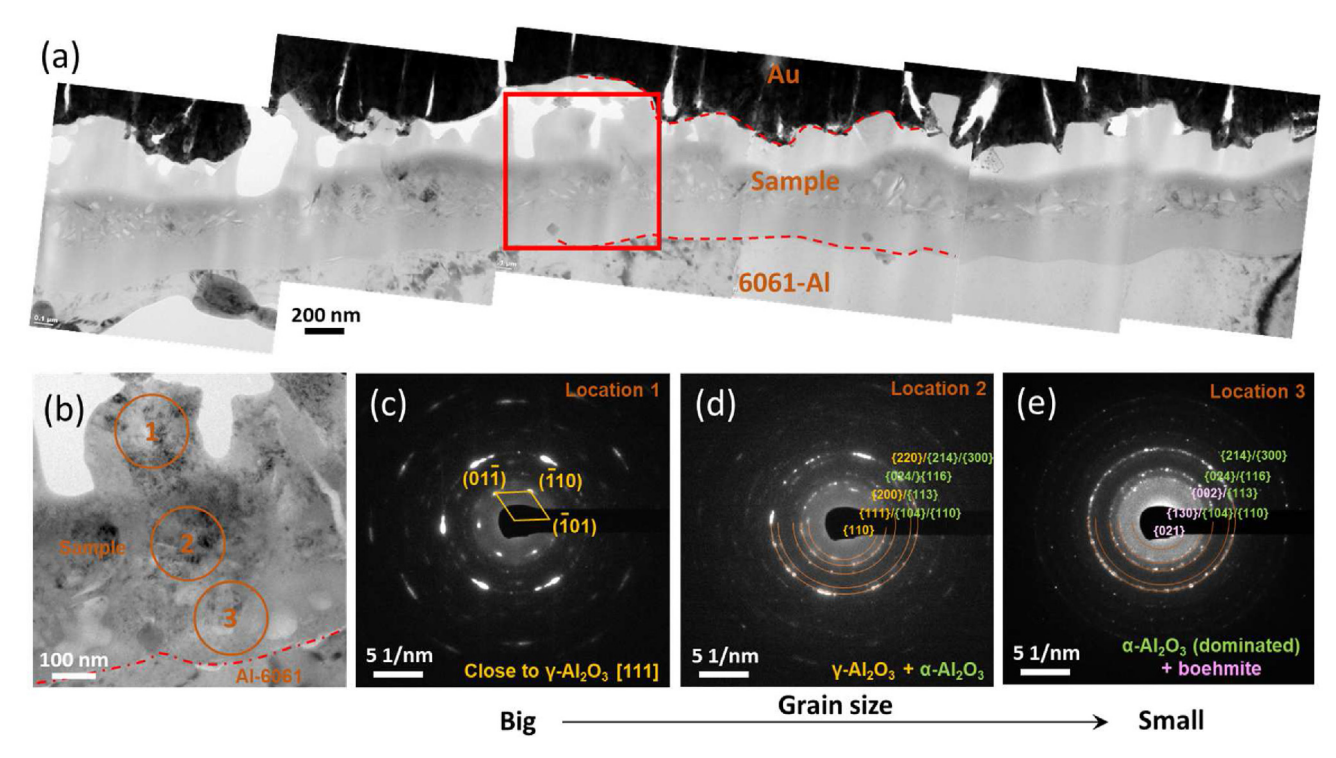


Fig. 4 - (a) BF-TEM images showing a cross section of the alkaline-etched, boehmite coated coupon; (b) BF-TEM image of the red boxed area in (a). (c)–(e) SAED patterns of locations 1–3 in (b), respectively.

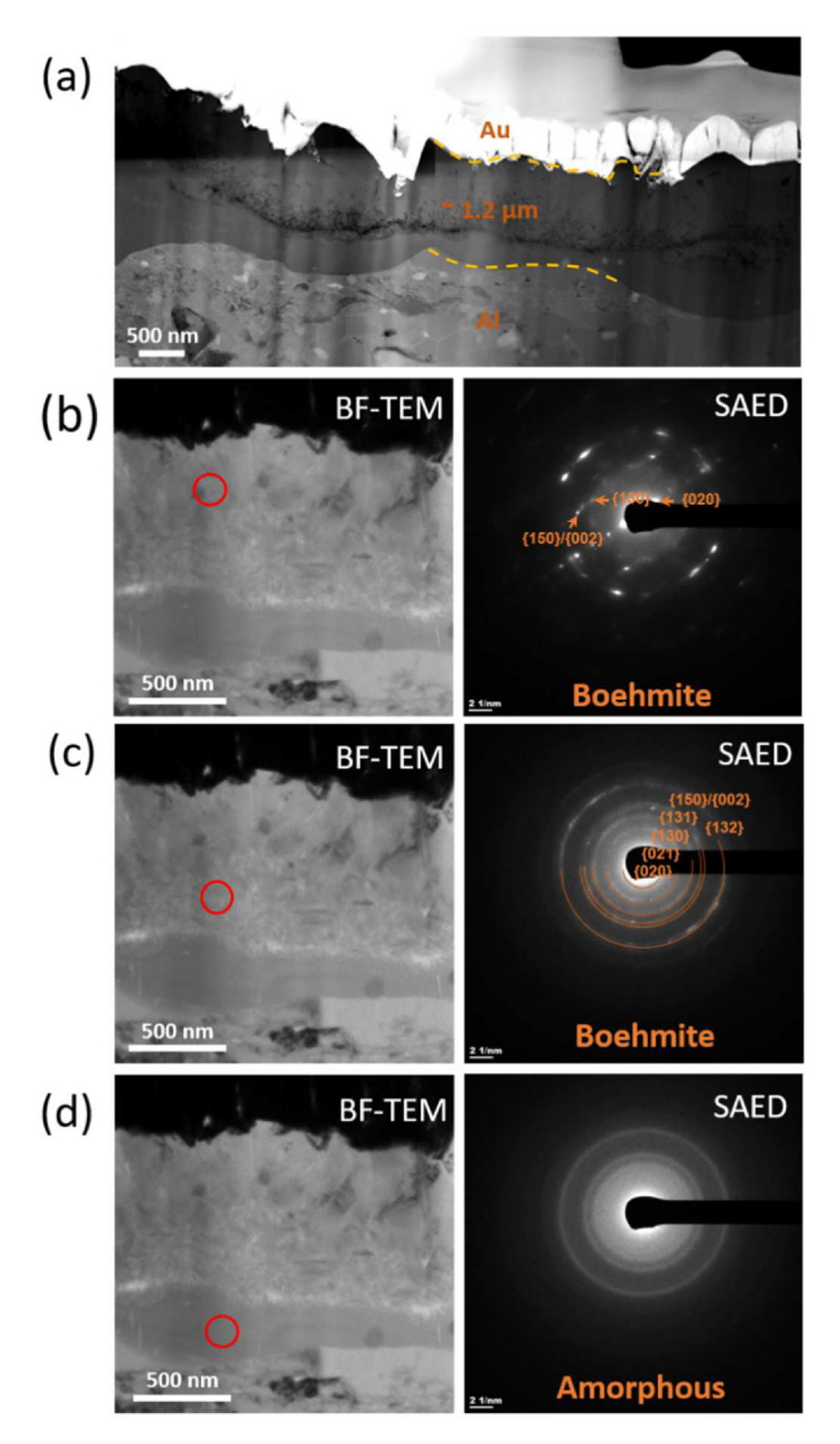


Fig. 5 - (a) Bright-field (BF) TEM image showing the cross section of the as-polished boehmite coated coupon; (b,c,d) BF-TEM images (left) and corresponding SAED images (right) of the areas circled in red.

at 285.0 eV that is reduced significantly during the etching cycle. Furthermore, the O/Al ratio is close to 4.5 before etching, which indicates that the oxide contribution to the aluminum oxide (from C-O and C=O bonds in the contamination) is overestimated at the surface that is etched away after the first

etching cycle. The peak area ratio of O/Al (Fig. 2d) remains stable around 2 after the first etching cycle, which is consistent with the boehmite structure of AlO(OH). After the second etching, the ratio slowly decreased to 1.75. This ratio is slightly lower than the expected stoichiometry for the boehmite but

higher than that of the ${\rm Al_2O_3}$. This result is likely a result of preferential sputtering of oxygen that occurred during etching. The XPS depth profile results are similar to the polished boehmite sample shows similar results (Fig. 3) with a slight increase after 80 nm that is likely due to an amorphous region that exists close to the AA6061 interface that could contain alumina.

3.2. TEM-SAED and GI-XRD

Microstructure of the sample was further investigated by TEM for the alkaline-etched and as-polished boehmite coupons (Figs. 4 and 5, respectively). The average thickness of the sample is 680 ± 110 nm (Fig. 4a). SAED patterns (Fig. 5b and c) show that the topmost surface ($<\sim$ 280 nm) is dominated by γ - Al_2O_3 with a grain size of 146 \pm 20 nm. The subsurface (~280–480 nm, Figs. 5b and 3d) consists of mixed lamellar α and γ -Al₂O₃ and phases with a grain size ~16.9 nm \times 75.0 nm. The bottom of the sample (~480–680 nm, Figs. 4b-3e) is dominated by α -Al₂O₃ along with a few weak boehmite diffraction spots (Fig. 5e) with a grain size of ~5 nm. However, it is possible that the surface could contain amorphous boehmite (or very little crystalline boehmite) with a dominating Al₂O₃ diffraction signal. SAED may also not have detected boehmite at the surface of the coupon because the analysis area is small (20 μm as compared 400 $\mu m \times$ 400 μm for XPS). The as-polished boehmite coupon has a thicker boehmite layer (~1.2 μm) than the alkaline etched coupon and also has amorphous SAED patterns close to the interface with AA6061 (Fig. 5). However, near the surface, crystalline boehmite was detected. This suggests that the pretreatment of the surface greatly affects the characteristics of the interface between the boehmite layer and AA6061. Lastly, an important note about the SAED results includes past reports of the decomposition of boehmite upon electron beam irradiation [23,24]. However, this work did not indicate such decomposition since crystalline boehmite was detected in both the polished and alkaline etched samples, which may be due to the rigid nature of the cladding vs the powder since the decomposition mechanism originates from surface hydroxyl groups. Aluminum oxide particles was only detected in the alkaline-etched coupon (Figs. 4 and 5) which also verified insignificant effect of boehmite decomposition under electron beam, considering that similar SAED imaging conditions of both samples were employed.

The interfacial boehmite was further investigated using GI-XRD in Fig. 6 to obtain characteristics of the bulk material to complement those of the surface in the SAED results. The diffraction patterns of both the alkaline-etched and the aspolished coupons show strong boehmite diffraction peaks as well as some metallic aluminum peaks, which likely are from the AA6061 that is underneath the boehmite layer. The aspolished boehmite, however, shows small peaks that match $\alpha\text{-Al}_2O_3$. The SAED results in Fig. 5 do not indicate boehmite in the cross section of the sample. However, the $\alpha\text{-Al}_2O_3$ could be present in other places throughout the layer, such as the AA6061 substrate, that the alkaline etching treatment could have etched away. The $\alpha\text{-Al}_2O_3$ peaks could also have originated from the AA6061 surface underneath the boehmite since for the grazing incidence geometry employed we

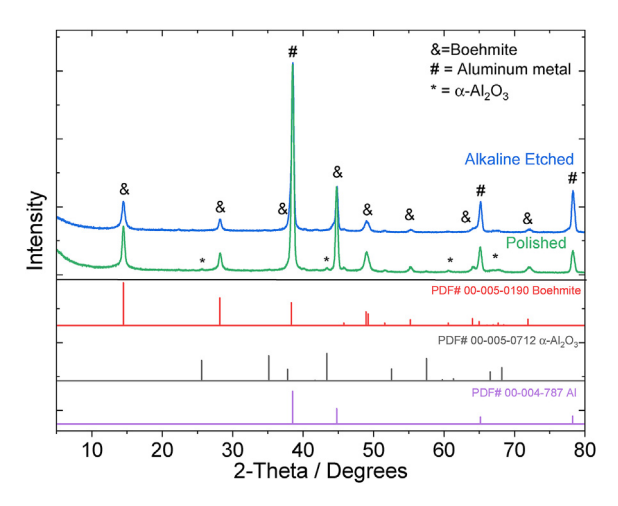


Fig. 6 – GI-XRD patterns obtained for the alkaline-etched and as-polished boehmite coupons with PDF references shown below. Both the as-polished and alkaline-etched samples show strong boehmite diffraction patterns. However, the polished boehmite shows minor peaks associated with α -Al₂O₃ that likely originated in the AA6061 along with Al peaks that originate from the underlying AA6061.

calculated that 90% of the x-rays would penetrate a 4.7 μm thick boehmite film. This may suggest that the alkaline etching treatment eliminated the original oxide layer on the AA6061. Furthermore, the alkaline-etched sample, which shows a mix of α - and $\gamma\text{-Al}_2O_3$ in the SAED, does not exhibit peaks matching $\alpha\text{-Al}_2O_3$ or $\gamma\text{-Al}_2O_3$. This could indicate that the amounts of these phases present on the surface are small and cannot be detected using GI-XRD. Additionally, the mechanical polishing belt used to polish the AA6061 could have left Al $_2O_3$ from the abrasive that was then etched away using the alkaline solution, which would explain the absence of the Al $_2O_3$ peaks in the GI-XRD pattern for the alkaline etched sample.

4. Discussion

To examine the surface chemical composition of the aspolished and alkaline-etched boehmite coupons, XPS was used due to its ability to identify oxidation states as well as approximate Al:O ratios. The XPS depth profile suggests some oxidation of the surface by a shift in the Al(2p) narrow scan region to a higher binding energy associated with boehmite in etching cycles after the initial etching process. The TEM-SAED results revealed a mix of α - and γ -Al₂O₃ on three different spots on the alkaline-etched sample. The aspolished boehmite, however, shows a mix of amorphous and crystalline boehmite in the SAED results. The GI-XRD data show some weak α-Al₂O₃ peaks in the as-polished boehmite that were not detected in the SAED results, which could be a result of it not being homogeneously dispersed throughout the boehmite layer. GI-XRD examines a much larger area of the surface than SAED does. Furthermore, the penetration depth of the x-rays in GI-XRD is about 4.5 μm , which suggests the α -Al $_2$ O $_3$ peaks could originate in the AA6061 substrate. This suggests that the alkaline etching treatment may have removed some of the AA6061 oxide. Additionally, the oxidation trend observed for the as-polished coupon but not in the etched coupon could be a result of formation anions left on the surface that the alkaline etching was able to eliminate. These ionic impurities have been shown to decrease the stability of the boehmite layer, which could have amorphized the boehmite seen in the TEM results [16]. Furthermore, the etching technique likely removed residual Al $_2$ O $_3$ from the abrasive used for the mechanical polishing, which is evident from the lack of Al $_2$ O $_3$ peaks in the GI-XRD pattern for the alkaline etched sample.

5. Conclusions

In this work, we investigated the chemical changes of the boehmite layer resulting specifically from alkaline pretreatment of the AA6061 surface prior to boehmite formation. Multimodal analysis including XPS, TEM, and GI-XRD provided an in-depth view of the chemical composition and morphology of the boehmite layer present after alkaline etching pretreatment. XPS depth profiling results indicate a potential oxidation layer at the surface of the alkaline treated boehmite coupon that diminishes after etching (indicated by a shift in the Al(2p) peak). TEM-SAED examination found a mix of α - and γ -Al₂O₃ in the alkaline-etched coupon, whereas only boehmite was observed in the as-polished samples. The GI-XRD results indicated the presence of boehmite in both the as-polished and alkaline-etched samples. However, a small amount of α -Al₂O₃ was observed in the as-polished sample, which could have formed when some of the oxide layer on the AA6061 substrate was etched away during the alkaline treatment. Use of a multimodal analysis approach to identify the chemical changes the boehmite surface undergoes as a result of pretreatment of AA6061 suggests that alkaline etching of the surface produces more oxidation than polishing alone. Further work will investigate the effects of acid etching techniques on AA6061 as well as the electrochemical corrosion properties that wet etching techniques (alkaline and acid) have on the electronic properties associated with the boehmite layer.

Author contributions

V.V.J., R.S. and L.S. conceived the idea, M.S. performed the TEM work and analysis, V.S. performed the XPS studies, M. B and Q.M. performed the XRD analysis and aided in data interpretation. L.S. did the analysis and compiled all the results. All authors contributed to drafting or revising the paper. V.V.J. and R. S. supervised the work.

Funding

This work was supported by the U.S. Department of Energy (DOE) National Nuclear Security Administration's Office of

Materials Management and Minimization (M3) under Contract DE-AC05-76RL01830.

Declaration of Competing Interest

The authors declare that they have no known competing financial interests or personal relationships that could have appeared to influence the work reported in this paper.

Acknowledgments

In addition to support from the DOE National Nuclear Security Administration, The authors are grateful for administrative support from Ms. Karrie Clark and to Paul Martin for acquiring supplies and consumables. The authors thank Anthony Guzman, Michael Blazon and Alan Schemer-Kohrn of Pacific Northwest National Laboratory (PNNL) for assisting in the metallographic sample preparation, and all the other staff directly or indirectly associated with producing the results featured in this publication.

The research was performed using the facilities at the Environmental Molecular Sciences Laboratory, a national scientific user facility sponsored by the DOE's Biological and Environmental Research program and located at PNNL.

REFERENCES

- [1] Meyer MK, Hofman GL, Hayes SL, Clark CR, Wiencek TC, Snelgrove JL, et al. Low-temperature irradiation behavior of uranium-molybdenum alloy dispersion fuel. J Nucl Mater 2002;304(1-3):221-36. https://www.sciencedirect.com/ science/article/pii/S0022311502008504.
- [2] Ozaltun H, Shen MHH, Medvedev P. Assessment of residual stresses on U10Mo alloy based monolithic mini-plates during Hot Isostatic Pressing. J Nucl Mater 2011;419(1–3):76–84. https://www.sciencedirect.com/science/article/pii/ S0022311511008063?via%3Dihub.
- [3] Senor DJ, Burks DE. Fuel fabrication capability research and development plan. Richland, Washington: Pacific Northwest National Laboratory; 2014. PNNL-22528, https://www.pnnl. gov/main/publications/external/technical_reports/PNNL-22528Rev1.pdf.
- [4] Meyer MK, Keiser DD, Jue J-F, Shaber E. Research reactor fuels. In: Advances in nuclear fuel chemistry; 2020. p. 273–312
- [5] Ajantiwalay T, Smith C, Keiser DD, Aitkaliyeva A. A critical review of the microstructure of U—Mo fuels. J Nucl Mater 2020;540:152386.
- [6] Nyberg EA, Joshi VV, Lavender CA, Paxton DM, Burks DE. The influence of casting conditions of the microstructure of ascast U-10Mo alloys: characterization of the casting process baseline. Richland, Washington: Pacific Northwest National Laboratory; 2013. PNNL-23049, https://www.pnnl.gov/main/ publications/external/technical_reports/PNNL-23049.pdf.
- [7] Nyberg EA, Joshi VV, Lavender CA, Paxton DM, Burkes DE. Influence of homogenization on the mechanical properties and microstructure of the U-10Mo alloy, PNNL-23348. Richland, Washington: Pacific Northwest National Laboratory; 2014. https://www.pnnl.gov/main/publications/ external/technical_reports/PNNL-23348.pdf.

- [8] Kim YS, Chae HT, Van den Berghe S, Leenaers A, Kuzminov V, Yacout AM. Aluminum cladding oxide growth prediction for high flux research reactors. J Nucl Mater 2020;529:151926. https://www.sciencedirect.com/science/ article/pii/S0022311519310190?via%3Dihub.
- [9] Petrovic J, Thomas G. Reaction of aluminum with water to produce hydrogen. U.S. Department of Energy; 2008. https:// www1.eere.energy.gov/hydrogenandfuelcells/pdfs/ aluminium_water_hydrogen.pd.
- [10] Nabhan D, Kapusta B, Billaud P, Colas K, Hamon D, Dacheux N. Effects of pH, surface finish and thermal treatment on the corrosion of AlFeNi aluminum alloy. Characterization of oxide layers. J Nucl Mater 2015;457:196—204. https://www.sciencedirect.com/science/ article/pii/S0022311514007077.
- [11] Kim YS, Hofman GL, Robinson AB, Snelgrove JL, Hanan N. Oxidation of aluminum alloy cladding for research and test reactor fuel. J Nucl Mater 2008;378(2):220–8. https://www. sciencedirect.com/science/article/pii/S0022311508003590.
- [12] Lopez C, Galmes B, Soberats B, Frontera A, Rotger C, Costa A. Surface modification of pseudoboehmite-coated aluminum plates with squaramic acid amphiphiles. ACS Omega 2019;4(12):14868-74. https://www.ncbi.nlm.nih.gov/ pubmed/31552326.
- [13] Zhao Y, Frost RL, Martens WN, Zhu HY. Growth and surface properties of boehmite nanofibers and nanotubes at low temperatures using a hydrothermal synthesis route. Langmuir 2007;23(19):9850–9. https://www.ncbi.nlm.nih. gov/pubmed/17705405.
- [14] Wefers K, Misra C. Oxides and hydroxides of aluminum. 1987. Alocoa Laboratories, https://www.worldcat.org/title/ oxides-and-hydroxides-of-aluminum/oclc/18997314.
- [15] Bower JO, Glazoff MV, Eiden TJ, Rezvoi AV. Evaluation of erosion of the dummy "EE" plate 19 in YA type ATR fuel

- element during reactor PALM cycles. Idaho Falls, ID: Idaho National Laboratories; 2016. https://www.osti.gov/servlets/purl/1333230.
- [16] Shaber E, Hofman G. Corrosion minimization for research reactor fuel. Idaho Falls, ID: Idaho National Laboratory; 2005. https://inldigitallibrary.inl.gov/sites/sti/3028321.pdf.
- [17] Rotole JA, Sherwood PMA. Gibbsite (α-Al(OH)₃) by XPS. Surf Sci Spectra 1998;5(1):25–31. https://avs.scitation.org/doi/10. 1116/1.1247853.
- [18] Rotole JA, Sherwood PMA. Nordstrandite (Al(OH)₃) by XPS. Surf Sci Spectra 1998;5(1):32–8. https://doi.org/10.1116/ 1.1247854.
- [19] Rotole JA, Sherwood PMA. Gamma-alumina (γ-Al₂O₃) by XPS. Surf Sci Spectra 1998;5(1):18–24. https://avs.scitation.org/ doi/10.1116/1.1247852.
- [20] Rotole JA, Sherwood PMA. Corrundum (α -Al₂O₃) by XPS. Surf Sci Spectra 1998;5(1):11–7. https://doi.org/10.1116/1.1247851.
- [21] Rotole JA, Sherwood PMA. Boehmite (γ-AlOOH) by XPS. Surf Sci Spectra 1998;5(1):53–9. https://doi.org/10.1116/ 1.1247857
- [22] Oswald S, Thoss F, Zier M, Hoffmann M, Jaumann T, Herklotz M, et al. Binding energy referencing for XPS in alkali metal-based battery materials research (II): application to complex composite electrodes. Batteries 2018;4(3):36.
- [23] Mergelsberg ST, Dembowski M, Bowden ME, Graham TR, Prange M, Wang HW, et al. Cluster defects in gibbsite nanoplates grown at acidic to neutral pH. Nanoscale 2021;13(41):17373–85. https://www.ncbi.nlm.nih.gov/ pubmed/34713874.
- [24] Sassi M, Walter ED, Qafoku O, Rosso KM, Wang Z. Radiationinduced interfacial hydroxyl transformation on boehmite and gibbsite basal surfaces. J Phys Chem C 2020;124(40):22185–91.